Nanoscale

ROYAL SOCIETY OF CHEMISTRY

PAPER

View Article Online
View Journal | View Issue

Cite this: *Nanoscale*, 2023, **15**, 13102

Control over product formation and thermodynamic stability of thiolate-protected gold nanoclusters through tuning of surface protecting ligands†

Manju P. Maman,[a] Eyyakkandy Nida Nahan,[a] Greeshma Suresh,[a] Arunendu Das,[b] Akhil S. Nair,[b] Biswarup Pathak[b] and Sukhendu Mandal*[a]

Received 3rd June 2023,
Accepted 5th July 2023

DOI: 10.1039/d3nr02617e

rsc.li/nanoscale

Surface-protecting ligands can regulate the structure of a cluster's core either through electronic or steric effects. However, the influence of the steric effect along with the electronic effect over controlling the structure during ligand exchange reactions remains elusive. To understand this, we have carried out ligand exchange on $[Au_{23}(CHT)_{16}]^-$ (CHT: cyclohexane thiol) using aromatic thiolates where we have tuned the bulkiness at the *para* position of the thiolate group on the incoming ligands. The outcome of the experiments reveals that each of the ligands in the chosen series is precisely selective towards the parent cluster transformation through specific intermediates. The ligand with more steric crowding directed the reaction pathway to have Au_{28} nanocluster as the major product while Au_{36} was the final product obtained with the gradual decrease of bulkiness over the ligand. The combined experimental and theoretical results elucidated the mechanism of the reaction pathways, product formation, and their stability. Indeed, this study with the series of ligands will add up to the ligand library, where we can decide on the ligand to obtain our desired cluster for specific applications through the ligand exchange reaction.

Introduction

Surface-protecting organic ligands in inorganic nanomaterials, like metal nanoparticles or metal nanoclusters (NCs), provide stability to the clusters from aggregation and thereby control the interparticle interactions.[1–4] The role of ligands becomes more crucial and emanant as the size of the metal NCs decreases. For instance, in the case of metal NCs with a size less than 2 nm, the presence of a ligand influences the structure because of the quantum confinement effect, and it also controls the high surface energy of bare NCs. This affects the physico-chemical properties and reactivity of the metal NCs as they are very sensitive to their structures/size.[5–9] The ligand exchange reaction (LER) is one of the best strategies to understand the ligand effect in changing the structure of metal nanoclusters.[10–15] Particularly, LER has gained much attention in thiolated gold NCs because of their fascinating structural and physico-chemical properties that vary upon surface modification.[16–19] For example, the optical properties of $Au_{25}(SR)_{18}$ were tuned through ligand exchange, and this happened due to the structural deformation of the parent cluster.[20] The LER strategy is not only used to introduce new properties, but it also has been used as a probe to obtain mechanistic insights into structural changes.[21–23] The knowledge of ligand parameters that influence the transformation of the parent cluster during the ligand exchange reaction will help us provide an insight into its mechanism, which will be beneficial for designing a new cluster with desired properties. Currently, there are some progress on the mechanistic aspect of LERs.[24–26] However, in view of the fact that surface-protecting ligands can exchange between the formed clusters, the material nature is quite dynamic.[27] So, a detailed elucidation of the ligand-exchange reaction in an atom-precise manner with control in position and the number of incoming ligands remains challenging.

Single crystal structure analysis revealed that thiolate-protected gold-nanoclusters can be represented as $Au_n(SR)_m$ (where n and m represent the number of gold and thiolate ligands, respectively) and contain the Au(0) core that is protected by the Au(I)-thiolate staple motif.[28,29] The variability in the staple motif is crucial for the ligand exchange as the reactivity depends on the binding energy of the respective staple motif.[30] For example, the $[Au_{23}(SR)_{16}]^-$ nanocluster consists of

[a]*School of Chemistry, Indian Institute of Science Education and Research Thiruvananthapuram, Kerala 695551, India. E-mail: sukhendu@iisertvm.ac.in*
[b]*Department of Chemistry, Indian Institute of Technology, Indore, Madhya Pradesh 453552, India*

† Electronic supplementary information (ESI) available. See DOI: https://doi.org/10.1039/d3nr02617e

three types of staple motifs, *i.e.*, dimer $[Au_2(SR)_3]$, monomer $[Au(SR)_2]$, and bridging thiolates [–S–] which protect the Au_{15} kernel of the Au_{23} NC.[31] Here, the core of the Au_{23} NC is a cuboctahedron in the presence of two extra hub Au atoms.[31] Therefore, the influence of steric and electronic effects of the ligand is expected to be different during ligand exchange reactions at different positions.[32] The process of ligand exchange can directly influence the core size and the extent of the reaction can regulate the surface environment of the metal nanoclusters.

Recently, we have conducted the ligand exchange reaction on $[Au_{23}(CHT)_{16}]^-$ using aromatic and bulky ligands.[32,33] Aromatic ligands led to $Au_{25}(SR)_{18}$ cluster formation and the bulkiness of the aromatic ligands led to $Au_{28}(SR)_{20}$ cluster formation. A detailed mechanistic study revealed that the bulky 4-TBBT (4-*tert*-butylbenzenethiol) ligand leads to complete ligand exchange and simultaneously induces size conversion to the $Au_{28}(SR)_{20}$ cluster, which ultimately undergoes size growth to form the $Au_{36}(SR)_{24}$ nanocluster.[33] Periodic growth of gold cores through continuous growth of the Au_4 tetrahedral unit leads to the formation of the Au_{36} cluster from the Au_{28} cluster.[34] In the case of the aromatic thiol ligand, bridging thiolates and hub gold atoms took part in the transformation process and contributed to the formation of the icosahedron kernel in the $Au_{25}(SR)_{18}$ cluster.[33] Apart from the thermodynamic stability differences, the specificity of the ligands towards different staple motifs could impact this transformation.[33,35] There is no systematic directive on the influence of the electronic and steric effects of the ligands during ligand exchange on stable Au_{23} NC. Specifically, precise control over the product selectivity through ligand exchange is yet to be achieved.

In this report, we have tried to understand the role of the bulky alkyl group (R) at the *para* position of the aromatic thiolate ligand in core selectivity. For this, we tuned the alkyl (R) group at the *para* position of the aromatic thiolate ligand and carried out ligand exchange in the $[Au_{23}(CHT)_{16}]^-$ nanocluster with five different ligands (Scheme 1). Herein, we observed that the aromaticity (electronic effect) and a slight change in the bulkiness of the incoming ligand (steric effect) have a greater influence over the core selectivity and stability of the products.

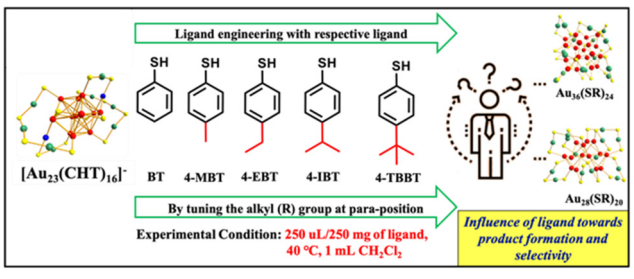

Scheme 1 Role of the ligand towards size/structural evolution of $[Au_{23}(CHT)_{16}]^-$ *via* ligand exchange where BT: benzenethiol, 4-MBT: 4-methylbezenethiol, 4-EBT: 4-ethylbenzenethiol, 4-IBT: 4-iso-propylbenzenethiol, 4-TBBT: 4-*tert*-butylbenzenethiol.

Results and discussion

Transformation of the $[Au_{23}(CHT)_{16}]^-$ nanocluster *via* ligand exchange was carried out with the given ligands (Scheme 1), where we tuned the bulkiness of the substituent on the *para* position of the benezenethiol ligand.

Case of 4-TBBT

At the initial stage of the time-dependent MALDI-MS, a single peak depicting the $[Au_{23}(CHT)_{16}]^-$ nanocluster converted into a group of peaks with a consistent mass difference of 50 Da indicating successful ligand exchange over the Au_{23} nanocluster (Fig. 1). As the reaction proceeds further complete ligand exchange in the Au_{23} nanocluster was observed as depicted by an intense peak at 7171.4 *m*/*z* at 0.5 h which corresponds to Au_{23}(4-TBBT)$_{16}$. Indicating that the 4-TBBT ligand prefers to transform the parent cluster into the Au_{23}(4-TBBT)$_{16}$ nanocluster, majorly. Later (from 1 h to 24 h), Au_{23}(4-TBBT)$_{16}$ was found to be transforming majorly into the Au_{28}(4-TBBT)$_{19}$ nanocluster as a peak at 8656.3 *m*/*z* was noticed with the disappearance of the Au_{23}(4-TBBT)$_{16}$ nanocluster peak. Ultimately after 48 h, we found two intense peaks at 8656.3 *m*/*z* and 4937 *m*/*z* that correspond to the Au_{28}(4-TBBT)$_{19}$ nanocluster and the Au_{15}(4-TBBT)$_{12}$ gold complex, respectively. During the reaction, we observed Au_{25} and Au_{20} nanoclusters were formed as side products while the specific core selection occurred *via* 4-TBBT ligand exchange. Here, the peak obtained for Au_{15}(4-TBBT)$_{12}$ in the time-dependent MALDI-MS spectra is actually an in-source mass-analyzed adduct of Au_{10}(4-TBBT)$_{10}$ indicating that Au_{15}(4-TBBT)$_{12}$ is an Au_{10}(4-TBBT)$_{10}$

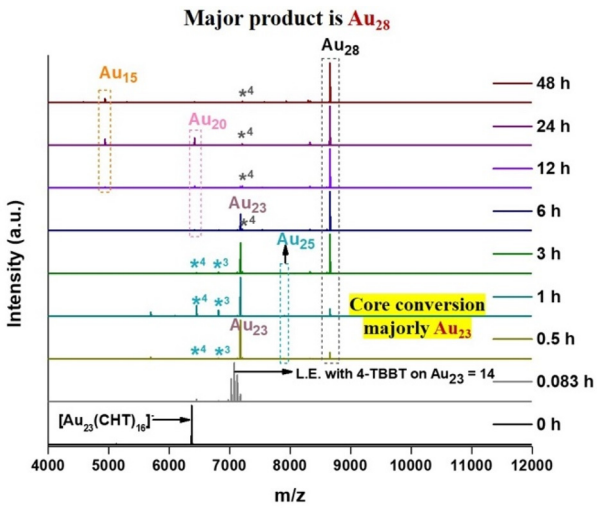

Fig. 1 Time-dependent MALDI-MS spectra showing the transformation process of the $[Au_{23}(CHT)_{16}]^-$ nanocluster during the ligand exchange with the 4-TBBT ligand. Note: magenta: $Au_{23}(SR)_{16}$ nanocluster, cyan: $Au_{25}(SR)_{18}$ and its fragment, black: $Au_{28}(SR)_{19}$ nanocluster and its fragment, pink: $Au_{20}(SR)_{15}$ nanocluster and its fragment, orange: Au_{15} nanocluster and its fragment. SR denotes the 4-TBBT ligand. (*) Asterisks represent the loss of AuL fragments, where the number with the asterisk represents how many AuL fragments are lost from the respective nanoclusters.

gold–thiol complex.[36] This is further supported by UV-visible spectroscopy and electrospray ionization-mass spectrometry (ESI-MS) data (Fig. S1†). Similarly, the peak of $Au_{28}(SR)_{19}$ corresponds to that of the $Au_{28}(SR)_{20}$ cluster, which observed with a loss of one ligand in MALDI-MS is caused by the labile nature of the aromatic ligand.[33,37]

Case of BT

At the initial stage, 0 to 1 h in time-dependent MALDI-MS, an intense peak at 5665 *m*/*z* that corresponds to the loss of an Au_4L_4 fragment from the $Au_{25}(BT)_{18}$ nanocluster was observed (Fig. 2). It indicates that the parent nanocluster, *i.e.*, $[Au_{23}(CHT)_{16}]^-$ was found to be successfully transformed into the $Au_{25}(BT)_{18}$ nanocluster. As the reaction proceeded further from 1 h to 3 h, an intense peak at 4263 *m*/*z* was observed that corresponds to the $Au_{15}(BT)_{12}$ nanocluster. At the same time, we observed the disappearance of all the peaks corresponding to the Au_{25} nanocluster. This indicates either the Au_{25} nanocluster is transformed into another nanocluster or degraded to form the gold–thiol complex. Later, after 48 h, only one peak was observed at 8380 *m*/*z* which corresponds to the mass of $Au_{32}(BT)_{19}$ which is a fragment of the Au_{36} cluster formed due to the loss of the Au_4L_4 fragment from the single ligand lost $Au_{36}(BT)_{24}$ nanocluster. During the process, very less intense peaks of Au_{28}, Au_{20}, and Au_{15} nanoclusters were found, those are the side products during the specific core selection. For better understanding, the same transformation process was monitored in different mass ranges of the mass spectrometer (Fig. S2†). From 3 h to 48 h, we observed the disappearance of the Au_{25} nanocluster peak, and at the same time, we observed the peak emergence at 8380 *m*/*z* that corresponds to $Au_{32}(BT)_{19}$, formed due to the fragmentation of the Au_{36} cluster as same as the previous spectra (Fig. 2).

This clearly indicates that the Au_{25} nanocluster is involved in the formation of the Au_{36} nanocluster. Ultimately after 48 hours, only one peak was observed at 8380 *m*/*z* which corresponded to the loss of the Au_4L_4 fragment from the single ligand lost $Au_{36}(BT)_{24}$ nanocluster.

Here, in the case of $Au_{25}(SR)_{18}$, its Au_4L_4 fragment is found to be more pronounced in MALDI-MS spectra during transformation due to the stability of the fragment.[38] Similarly, in the case of the $Au_{36}(SR)_{24}$ nanocluster, the peak observed in MALDI-MS is recognized by the fragment peak corresponding to $Au_{32}(SR)_{19}$.[39]

It was observed from the above two cases that the core conversion of $[Au_{23}(CHT)_{16}]^-$ occurred either through the formation of Au_{23} or Au_{25}, which is completely determined by ligand parameters. The preference for core conversion towards $Au_{23}(SR)_{16}$ NC is more likely to occur when there is a bulky alkyl group on the benzenethiol, whereas when the bulkiness reduces, the core conversion towards the Au_{25} NC is more preferred. For 4-IBT, 4-EBT, and 4-MBT, both Au_{23} and Au_{25} NCs were observed, and their relative amount depends on the bulkiness of the respective ligand (Fig. 3).

The reaction mixture for each case was quenched, dried and further purified through size exclusion chromatography (SEC) and the bands obtained in each case were collected separately for quantification and further studies (for more information, see the ESI†). Qualitative analysis of each band was conducted using UV-visible spectroscopy and mass spectrometry (Fig. S3–S7†). In the case of 4-TBBT, 4-IBT, and 4-EBT, we observed three bands in SEC, which corresponds to $Au_{36}(SR)_{24}$ (band-1), $Au_{28}(SR)_{20}$ (band-2), and the $Au_{10}(SR)_{10}$ gold thiol complex (band-3) respectively (Fig. S3–S5†). While in the case of 4-MBT, we observed two bands, in which band-1 stands for $Au_{36}(SR)_{24}$ and band-2 stands for $Au_{10}(SR)_{10}$ (Fig. S6†). In the case of BT, we observed only one band which corresponds to the $Au_{36}(SR)_{24}$ nanocluster (Fig. S7†). Each band was carefully collected separately and the solvent was evaporated to dryness. The obtained products were quantified for respective cases (Table 1).

The quantification of products obtained in each case reveals that as the bulkiness of the alkyl group (R) at the *para*-position of the aromatic thiolate ligand increases, the formation of the Au_{28} nanocluster was found to be more pronounced. At the same time, a reverse trend was observed in the case of the Au_{36} nanocluster formation. In addition to this, we also observed two final products, namely Au_{28} and Au_{36} in the case of 4-TBBT, 4-IBT, and 4-EBT. To confirm any further transformation, the reaction was continued for 11 days by maintaining similar conditions for these three cases, and the quantification of the obtained product was done similarly. In the case of 4-IBT and 4-EBT, we could obtain only a single product which was confirmed to be Au_{36}, and in the case of 4-TBBT, it gave rise to three products as we observed at 48 hours (Table 2).

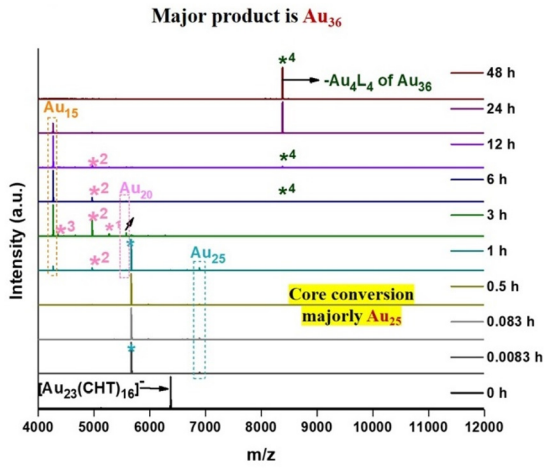

Fig. 2 Time-dependent MALDI-MS spectra showing the transformation process of the $[Au_{23}(CHT)_{16}]^-$ nanocluster during the ligand exchange with the BT ligand. Note: dark green: Au_{36} nanocluster and its fragment, cyan: $Au_{25}(SR)_{18}$ and its fragment, black: $Au_{28}(SR)_{19}$ nanocluster and its fragment, pink: $Au_{20}(SR)_{15}$ nanocluster and its fragment, orange: Au_{15} nanocluster and its fragment where SR denotes the BT ligand. (*) Asterisks represent the loss of the AuL fragment, where the number with the asterisk represents how many AuL fragments are lost from the respective nanoclusters.

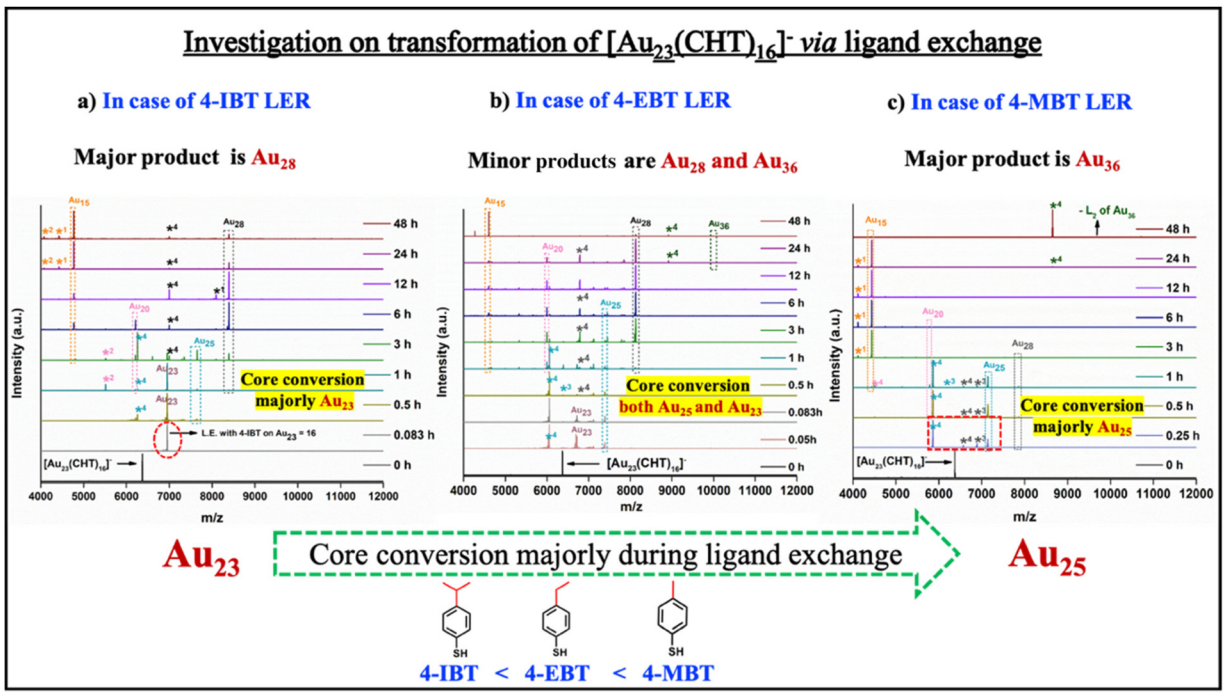

Fig. 3 Time-dependent MALDI-MS spectra showing the transformation process of the $[Au_{23}(CHT)_{16}]^-$ nanocluster during (a) 4-IBT ligand exchange, (b) 4-EBT ligand exchange, (c) 4-MBT ligand exchange. Note: dark green: Au_{36} nanocluster and its fragment, cyan: $Au_{25}(SR)_{18}$ and its fragment, pink: $Au_{20}(SR)_{15}$ nanocluster and its fragment, orange: Au_{15} nanocluster and its fragment. SR denotes 4-IBT, 4-EBT, and 4-MBT in the respective spectra. (*) Asterisks represent loss of the AuL fragment where the number with the asterisk represents how many AuL fragments are lost from the respective nanoclusters.

Table 1 Quantification of products obtained in the LERs after 48 h with respect to the parent $[Au_{23}(CHT)_{16}]^-$ nanocluster

Ligand (-SR)	BT	4-MBT	4-EBT	4-IBT	4-TBBT
Yield (%) of $Au_{36}(SR)_{24}$ w.r.t. precursor	25	17.8	12.8	8.3	~2
Yield (%) of $Au_{28}(SR)_{20}$ w.r.t. precursor	0	0	14	21	38.4
Yield (%) of $Au_{10}(SR)_{10}$ w.r.t. precursor	0	15.3	69.2	75.6	57.6

Table 2 Comparison of yield obtained at two different times as well as at the same time

Ligand	4-EBT	4-IBT	4-TBBT
Quantification of the products obtained after 48 hours			
Yield (%) of $Au_{36}(SR)_{24}$ w.r.t. precursor	12.8	8.3	~2
Yield (%) of $Au_{28}(SR)_{20}$ w.r.t. precursor	14	21	38.4
Yield (%) of $Au_{10}(SR)_{10}$ w.r.t. precursor	69.2	75.6	57.6
vs.			
Quantification of the products obtained after 11 days			
Yield (%) of $Au_{36}(SR)_{24}$ w.r.t. precursor	12.8	8.3	~2
Yield (%) of $Au_{28}(SR)_{20}$ w.r.t. precursor	0	0	23.4
Yield (%) of $Au_{10}(SR)_{10}$ w.r.t. precursor	0	0	71.7

The comparison of the percentage of the yield of the products obtained at 48 h with 11 days' reactions led to two main outcomes:

Point 1: No variation in the amount of the Au_{36} nanocluster even after 11 days indicated that the Au_{28} nanocluster was not involved in the formation of the Au_{36} nanocluster in any of the cases. This also suggested that the formation of Au_{28} and Au_{36} nanoclusters are from two different routes.

Point 2: In the case of 4-TBBT, the amount of the Au_{28} nanocluster was found to be decreased at the same time, we observed an increment in the amount of Au_{10}, indicating that Au_{28} degraded to form the gold–thiol complex. While in cases of 4-IBT and 4-EBT, we observed the decomposition of both the Au_{28} nanocluster and Au_{10} gold–thiol complex as the reaction proceeded. These results suggest that the bulkiness of the alkyl group favors Au_{28} nanocluster formation and provides stability.

The facts collected through the investigation of the transformation process and quantification of products after 48 hours (*i.e.*, from Schemes 2a and b, respectively), indicate that the formation of the Au_{28} nanocluster was caused by the transformation of the parent nanocluster through the $Au_{23}(SR)_{16}$ intermediate during ligand exchange (Scheme 2). Whereas the formation of the Au_{36} nanocluster was caused by the transformation of the parent nanocluster to the $Au_{25}(SR)_{18}$ intermediate (Scheme 2). This indicates that the selectivity and stability of a specific core during the ligand exchange are well governed by ligand parameters which is evident in this example.

The ligand effect over cluster stability

To understand the role of ligands on the stability of the obtained products, a stability test was done by heating the

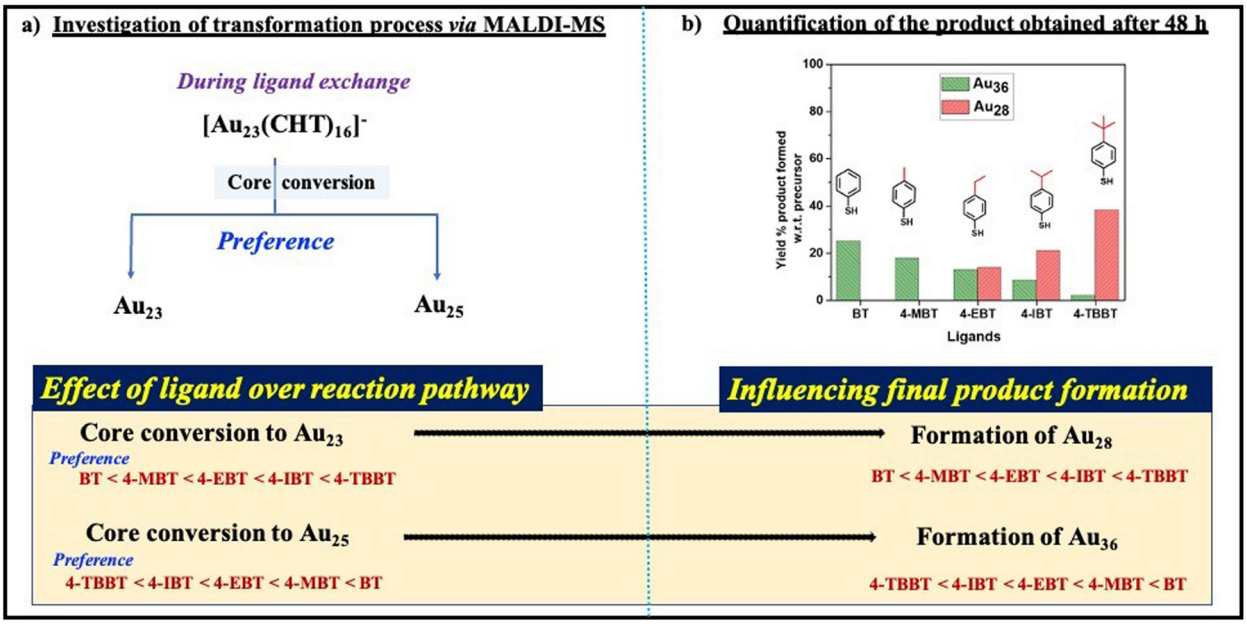

Scheme 2 (a) Summary of the product formation based on time-dependent MALDI-MS spectra obtained for the LER process on the $[Au_{23}(CHT)_{16}]^-$ nanocluster transformation with the series of ligands. (b) Summary obtained from the quantification of the product analysis for the $[Au_{23}(CHT)_{16}]^-$ nanocluster transformation process with the series of ligands.

solution of Au_{28} and Au_{36} clusters at 40 °C. The solution was characterized using UV-visible spectroscopy conducted over a period. The results obtained for $Au_{28}(SR)_{20}$ nanoclusters (where SR = 4-TBBT, 4-IBT, and 4-EBT respectively) is shown in Fig. 4.

In the case of 4-TBBT, the Au_{28} nanocluster was found to be stable even after one week. While in the case of 4-IBT, the UV-visible absorption spectra collected during the experiment changed after 72 hours, indicating less stability of Au_{28}(4-IBT)$_{20}$ compared to Au_{28}(4-TBBT)$_{20}$. For Au_{28}(4-EBT)$_{20}$, the UV-visible spectra changed after 12 hours indicating the least stability of Au_{28}(4-EBT)$_{20}$ among the three clusters. So, the trend obtained for the stability was found to be Au_{28}(4-TBBT)$_{20}$ > Au_{28}(4-IBT)$_{20}$ > Au_{28}(4-EBT)$_{20}$. It indicates that the bulkiness of the alkyl group at the *para* position of the aromatic thiolate ligand has a role in determining the stability of the Au_{28} cluster and it increases with the bulkiness.

The UV-Visible spectra showing the stability test of $Au_{36}(SR)_{24}$ are given in Fig. S8.† Similar to the case of $Au_{28}(SR)_{20}$ clusters, 4-TBBT-protected Au_{36} was the most stable among all the five clusters where the spectral features existed as such for more than 2 weeks. Whereas $Au_{36}(BT)_{24}$ was the least stable and started to degrade within 6 hours. The order of stability was found to be Au_{36}(4-TBBT)$_{24}$ > Au_{36}(4-IBT)$_{24}$ > Au_{36}(4-EBT)$_{24}$ > Au_{36}(4-MBT)$_{24}$ > $Au_{36}(BT)_{24}$. Here we could observe that even though the formation of the Au_{36} cluster is least preferred by the 4-TBBT ligand, Au_{36}(4-TBBT)$_{24}$ is the most stable cluster among all the $Au_{36}(SR)_{24}$ clusters. So, the

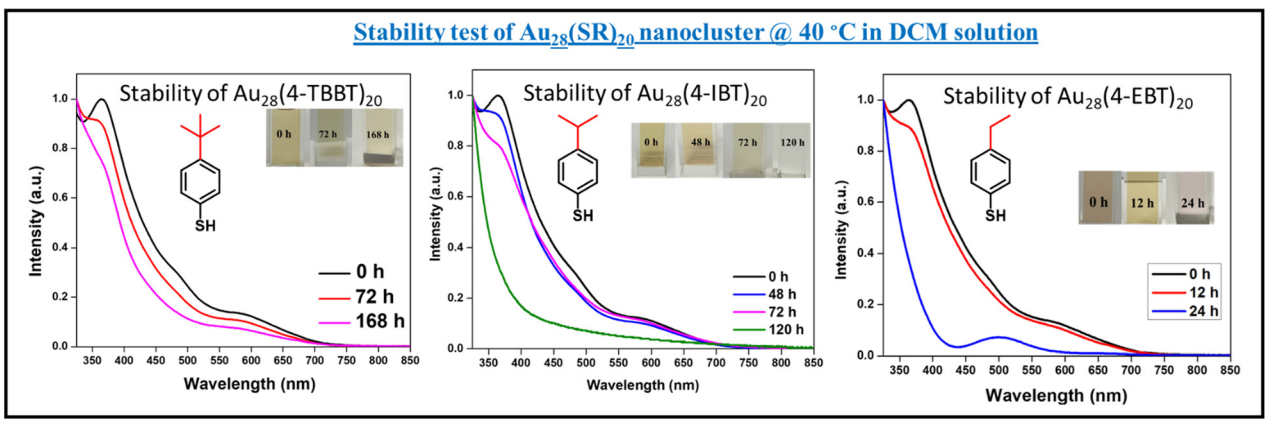

Fig. 4 UV-visible absorption spectra showing the stability test of $Au_{28}(SR)_{20}$.

ligands affect the reaction kinetics and stability of the clusters in a different way.

Theoretical calculations

To investigate the transformation pathway followed by the Au_{23} cluster during the TBBT ligand exchange, we carried out DFT calculations using the Vienna *ab initio* simulation package (VASP) (see Text S1 for computational details, Fig. S8 and S9†).[40] We infer that the structural and electronic differences in the gold–thiolate interfaces between the different clusters play an important role in determining the energetics of the ligand-assisted structural transformation. To investigate this, we analyzed average ligand removal reaction energy (LRE) for the TBBT ligand at different types of staples in these clusters (Text S1, eqn (1), Table S1 and Fig. S10†). Based on the LRE values, the ease of removal of the ligand follows an order of $Au_{25} > Au_{23} \sim Au_{28}$, where the latter two clusters differ by a negligible difference of 0.04 eV. We also calculated the formation energy of Au_{25} clusters with all the considered thiol ligands (Text S1, eqn (2) and Table S2†). The observed high formation energy values also infer less thermodynamic stability of TBBT with the Au_{25} cluster. This is in agreement with the experimental observation of the Au_{23} cluster favoring an initial TBBT ligand exchange without undergoing cluster transformation to Au_{25} as the latter is associated with less stability when bound to TBBT ligands. In addition, since the experimental results drive us to examine to what extent the various thiol ligands can stabilize Au_n clusters, we investigated this by conducting a case study of two aromatic thiols, 4-IBT (4-isopropylbenzenethiol) and 4-TBBT (4-*tert*-butylbenzenethiol).

In order to understand the role of a ligand over the specificity of the core selectivity, we calculated the barriers of rotation for 4-IBT and 4-TBBT ligands at the optimized Au_{25} geometry (Fig. S11, S12 and Table S3†). The rotational barrier is considered here as a metric for quantifying the bulkiness as it can be expected to have an inverse relationship with the extent of steric crowding imparted by the ligand bulkiness. We found that the ligand rotational barrier is very low in the case of 4-IBT compared to 4-TBBT which further supports the observation of Au_{25} becoming an important intermediate during the 4-IBT ligand exchange and not during the 4-TBBT ligand exchange.

To understand the intrinsic stability differences between the precursor and product clusters, we scrutinized the thermodynamic stability of the clusters. This was achieved by calculating the core cohesive energy (CE) and shell to core binding energy (CSBE) of all these clusters with different thiol ligands *via* the recently proposed thermodynamic stability criterion proposed by Mpourmpakis *et al.* (Text S1; eqn (3), (4) and Table S4†). We found that the CE and CSBE values of most of the individual clusters remain the same irrespective of the thiol ligand bulkiness. However, the observed high negative values of CE for the product cluster $Au_{36}(BT)_{24}$ trigger the core conversion through the structural transformation of the parent $[Au_{23}(CHT)_{16}]^-$ cluster. In this context, the energetics of all the transformation processes following eqn (5a)–(c) in Text S1† were investigated and their calculated reaction energy (RE) values for all thiol ligands are listed in Table S5.† The calculated high negative reaction energy of −6.01 eV for BT during the transformation again suggests that the reaction is energetically favorable, which can also be attributed to a more stable geometry of the $Au_{36}(BT)_{24}$ cluster. Also, the observed high negative reaction energy values among all the possible conversion processes indicate that Au_{25} is highly selective towards the Au_{36} cluster formation.

Furthermore, we also determined the average ligand interaction energy (LIE) of all the thiolate-protected parent and product clusters to understand the ligand effects and their selectivity toward a particular core present in these clusters. The LIE calculation method and their calculated values are given in Text S1 (eqn (6)) and Table S6,† respectively. It is observed that the interaction of thiol ligands in the Au_{28} and Au_{36} cluster is strong enough to retain the structural rigidity as evidenced by their high negative values of LIE in comparison with Au_{23} and Au_{25} clusters. The observed low negative values of LIE for Au_{23} and Au_{25} clusters clearly indicate weaker ligand interaction and also explain why these clusters prefer to undergo further transformations to higher congeners. On the basis of our CE and LIE values, we can understand that thiolate protected Au_{28} and Au_{36} clusters are more stable which supports their dominant presence in the MALDI-MS analysis of the ligand exchange process.

To further decouple the ligand *vs.* the core influence, we now attempted to correlate the RE values for the experimentally observed delayed core conversion during the ligand exchange with the observed factors such as CE, CSBE and LIE values of $[Au_{25}(SR)_{18}]^-$ clusters (Table S7†) during transformation from a theoretically proposed ligand exchange pathway. On the basis of calculated results, we found a significant correlation with average ligand interaction ($\sim R^2 = 0.72$) energy in comparison with those identified for CE and CSBE of the cluster. Since LIE is a parameter dominated by the ligand effect, it strongly implies that Au–SR interaction is a predominant factor for determining the kinetics of the transformation process as well as the stabilization of product clusters and hence turns out to be an effective factor influencing the cluster transformation (Table S6†). The order of favorability of the transformation of $[Au_{25}(SR)_{18}]^-$ clusters following Reaction-III (Text S1†) with varying bulkiness at the *para* position of the aromatic ligand (SR) was observed as BT > 4-MBT > 4-EBT ~ 4-IBT ~ 4-TBBT (Fig. S13†). Furthermore, we observed both LI and RE values decrease as the bulkiness in the thiol ligand increases during ligand exchange-assisted structural transformation to the Au_{36} cluster. It is noteworthy to mention that the trend in RE values for the conversion of the ligand exchanged Au_{23} cluster to the Au_{28} cluster are also in good agreement with the experimental findings (Table S5†). Therefore, we emphasized the effect of the bulkiness imparted by the ligand interaction with the particular core is a pivotal factor triggering the core conversion to form product clusters.

It has been observed in the experiment that the $Au_{36}(BT)_{24}$ nanocluster is formed from the parent cluster $[Au_{23}(CHT)_{16}]^-$ through the immediate formation of $[Au_{25}(BT)_{18}]^-$ without any signature of $Au_{28}(BT)_{20}$ *via* ligand exchange. This led us to

guide the mechanism of the transformation from $[Au_{23}(CHT)_{16}]^-$ to the Au_{36} *via* Au_{25} intermediate using ligand engineering (in the case of BT) in order to achieve coherence with the experimental scenario. It is to be noted that in our previous studies, we have reported mechanisms of higher symmetry Au_{23} to Au_{25} cluster formation through symmetry breaking of the core by the 2-NPT (2-naphthalenethiol) exchange and Au_{23} to Au_{28} transformation by the 4-TBBT exchange followed by size conversion through growth mechanism.[31,32] Here, we propose a two stage transformation process: stage-I, the transformation of Au_{23} to Au_{25} which was discussed in our previous studies and stage-II, the transformation of Au_{25} to Au_{36} is given in Scheme 3.

The proposed mechanism for the transformation of Au_{25} to Au_{36} by the cluster of clusters (COC) growth pathway is presented in Scheme 4. The initial step involves scissoring of dimeric staples causing the two icosahedral units (Au_{13} kernel) of Au_{25} to fuse together *via* edge linking [a, b]. After the fusion, a cluster of the Au_{26} kernel is formed with the combination of twelve $Au_2(SR)_3$ dimeric staples and dimeric rearrangement of dissociated fragments to form the Au_{20} core with eight dimers leaving the chair conformation (Fig. S14†) of the Au_6 unit (four dimers) during the process [c, d]. This is also supported by the sequential addition of two Au atoms to the remaining Au_6 (two Au_3 units) and four Au-SR units with four dimeric staples forming the theoretically derived $Au_{20}(SR)_{16}$ cluster and further disappearance of this cluster to form $Au_{15}(SR)_{13}$ as depicted in Fig. S15,† in accordance with the experimental observation (Fig. 2). The next step involves the exchange of eight dimeric staples *via* rotation followed by bond scissoring attached in the C_1 symmetry structure of the proposed Au_{20} core (d, e). Therefore, the core atoms can be considered to be performing the symmetry-assisted core rearrangement of the Au_{20} kernel (C_1 symmetry), which can undergo a later stage forming more symmetry (C_2) kernel *via* complex isomeric transition (Fig. S16†). This is followed by the combination of displaced core atoms with the layer-by-layer nature of the fcc kernel and thereby leads to the bond rearrangement of core atoms forming the higher symmetry isomeric Au_{20} kernel (f, g). Since the calculated negative values of CE of the Au_{20} kernel for the $Au_{36}(SR)_{24}$ cluster is much higher compared to $[Au_{25}(SR)_{18}]^-$ indicating that the core atoms are strongly bound

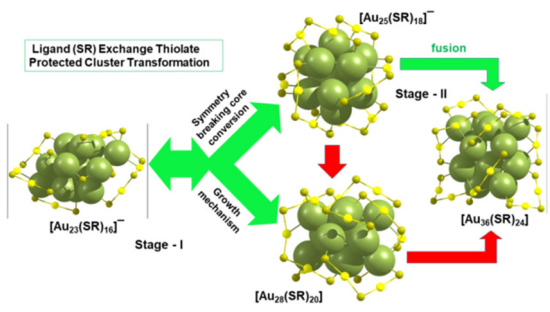

Scheme 3 Summary of the complete cluster transformation process from Au_{23} to Au_{36} *via* ligand exchange.

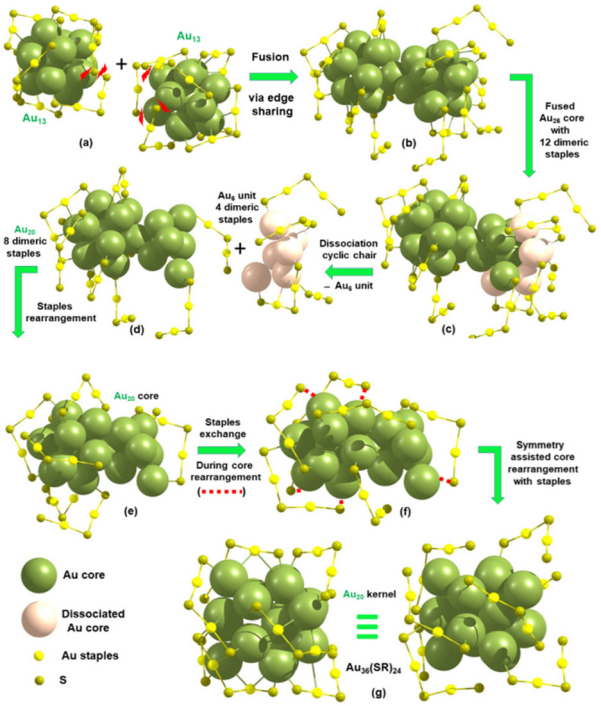

Scheme 4 The proposed mechanism for cluster transformation. (a and b) Scissoring dimeric staples in $Au_{25}(SR)_{18}$ clusters during fusion. (c, d and e) Dissociation of the cyclic chair conformation of the Au_6 unit from the fused Au_{26} core and staples rearrangement. (f and g) Isomeric core transition *via* the complex core rearrangement process towards the more symmetric Au_{20} kernel structure forming $Au_{36}(SR)_{24}$. The ligands are omitted for visual convenience.

to each other, the feasibility of the isomeric symmetry assisted core transition followed by dissociation of the cyclic Au_6 unit is expected to be the reliable pathway for the ligand exchange process studied in our work.

Conclusions

In summary, we have shown that the electronic effect and a variation in the steric effect of the incoming ligands have a crucial role in the size selectivity and preference of the pathway of transformation during the ligand exchange reaction. We observed that when the ligands have a bulkier substituent, $[Au_{23}(CHT)_{16}]^-$ preferred the transformation through the $Au_{23}(SR)_{16}$ intermediate which led to producing $Au_{28}(SR)_{20}$ as the major product. Whereas when the bulkiness gradually decreased, the reaction went through the pathway that favored the formation of the $Au_{36}(SR)_{24}$ cluster through the $Au_{25}(SR)_{18}$ intermediate. The influence of ligands in choosing the transformation pathway was evident from the gradual trend observed in the yield of the final products obtained. Steric crowding of the ligands not only dictates the pathway for the transformation, it also alters the stability of the clusters. A plausible mechanism based on symmetry-assisted isomeric core rearrangement is also proposed for Au_{25} to Au_{36} cluster

transformation. We envision that these results may add up to the resources of materials science to design new clusters of specific interest.

Data availability

The ESI contains experimental details, theoretical calculations, additional figures, tables and references.

Conflicts of interest

The authors declare no competing financial interest.

Acknowledgements

We acknowledge the funding support from the Science and Engineering Research Board, Govt. of India through the CRG/2022/000984 grant.

References

1 T.-H. Yang, Y. Shi, A. Janssen and Y. Xia, *Angew. Chem., Int. Ed.*, 2020, **59**, 15378–15401.
2 W. Suzuki, R. Takahata, Y. Chiga, S. Kikkawa, S. Yamazoe, Y. Mizuhata, N. Tokitoh and T. Teranishi, *J. Am. Chem. Soc.*, 2022, **144**, 12310–12320.
3 Y. Wang, J. E. Q. Quinsaat, T. Ono, M. Maeki, M. Tokeshi, T. Isono, K. Tajima, T. Satoh, S. Sato, Y. Miura and T. Yamamoto, *Nat. Commun.*, 2020, **11**, 6089.
4 Q. Tang, G. Hu, V. Fung and D. Jiang, *Acc. Chem. Res.*, 2018, **51**, 2793–2802.
5 M. W. Heaven, A. Dass, P. S. White, K. M. Holt and R. W. Murray, *J. Am. Chem. Soc.*, 2008, **130**, 3754–3755.
6 H. Shen, G. Deng, S. Kaappa, T. Tan, Y.-Z. Han, S. Malola, S.-C. Lin, B. K. Teo, H. Häkkinen and N. Zheng, *Angew. Chem., Int. Ed.*, 2019, **58**, 17731–17735.
7 J.-J. Li, Z.-J. Guan, Z. Lei, F. Hu and Q.-M. Wang, *Angew. Chem., Int. Ed.*, 2019, **58**, 1083–1087.
8 Y. Wang and T. Bürgi, *Nanoscale Adv.*, 2021, **3**, 2710–2727.
9 M. Zhu, C. M. Aikens, F. J. Hollander, G. C. Schatz and R. Jin, *J. Am. Chem. Soc.*, 2008, **130**, 5883–5885.
10 B. Zhang, J. Chen, Y. Cao, O. J. H. Chai and J. Xie, *Small*, 2021, **17**, 2004381.
11 R. Guo, Y. Song, G. Wang and R. W. Murray, *J. Am. Chem. Soc.*, 2005, **127**, 2752–2757.
12 E. S. Shibu, M. A. H. Muhammed, T. Tsukuda and T. Pradeep, *J. Phys. Chem. C*, 2008, **112**, 12168–12176.
13 C. L. Heinecke, T. W. Ni, S. Malola, V. Mäkinen, O. A. Wong, H. Häkkinen and C. J. Ackerson, *J. Am. Chem. Soc.*, 2012, **134**, 13316–13322.
14 A. Fernando and C. M. Aikens, *J. Phys. Chem. C*, 2015, **119**, 20179–20187.
15 Y. Shichibu, Y. Negishi, T. Tsukuda and T. Teranishi, *J. Am. Chem. Soc.*, 2005, **127**, 13464–13465.
16 Y. Chen, C. Liu, Q. Tang, C. Zeng, T. Higaki, A. Das, D. Jiang, N. L. Rosi and R. Jin, *J. Am. Chem. Soc.*, 2016, **138**, 1482–1485.
17 K. Pyo, H. Xu, S. M. Han, S. Saxena, S. Y. Yoon, G. Wiederrecht, G. Ramakrishna and D. Lee, *Small*, 2021, **17**, 2004836.
18 Y. Chen, M. Zhou, Q. Li, H. Gronlund and R. Jin, *Chem. Sci.*, 2020, **11**, 8176–8183.
19 Q. Tang, R. Ouyang, Z. Tian and D. Jiang, *Nanoscale*, 2015, **7**, 2225–2229.
20 A. Tlahuice-Flores, R. L. Whetten and M. Jose-Yacaman, *J. Phys. Chem. C*, 2013, **117**, 20867–20875.
21 Y. Li, R. Juarez-Mosqueda, Y. Song, Y. Zhang, J. Chai, G. Mpourmpakis and R. Jin, *Nanoscale*, 2020, **12**, 9423–9429.
22 Y. Song, H. Abroshan, J. Chai, X. Kang, H. J. Kim, M. Zhu and R. Jin, *Chem. Mater.*, 2017, **29**, 3055–3061.
23 C. Zeng, C. Liu, Y. Pei and R. Jin, *ACS Nano*, 2013, **7**, 6138–6145.
24 M. Rambukwella, N. A. Sakthivel, J. H. Delcamp, L. Sementa, A. Fortunelli and A. Dass, *Front. Chem.*, 2018, **6**, 1–17.
25 Y. Wang and T. Bürgi, *Nanoscale Adv.*, 2021, **3**, 2710–2727.
26 Y. Negishi, H. Horihata, A. Ebina, S. Miyajima, M. Nakamoto, A. Ikeda, T. Kawawaki and S. Hossain, *Chem. Sci.*, 2022, **13**, 5546–5556.
27 K. R. Krishnadas, A. Ghosh, A. Baksi, I. Chakraborty, G. Natarajan and T. Pradeep, *J. Am. Chem. Soc.*, 2016, **138**, 140–148.
28 Z. Ma, P. Wang, L. Xiong and Y. Pei, *Wiley Interdiscip. Rev.: Comput. Mol. Sci.*, 2017, **7**, e1315.
29 R. Jin and Y. Zhu, Atomically Precise Nanoclusters, Jenny Stanford Publishing, 2021.
30 C. Zeng, C. Liu, Y. Chen, N. L. Rosi and R. Jin, *J. Am. Chem. Soc.*, 2014, **136**, 11922–11925.
31 A. Das, T. Li, K. Nobusada, C. Zeng, N. L. Rosi and R. Jin, *J. Am. Chem. Soc.*, 2013, **135**, 18264–18267.
32 M. P. Maman, A. S. Nair, A. M. Abdul Hakkim Nazeeja, B. Pathak and S. Mandal, *J. Phys. Chem. Lett.*, 2020, **11**, 10052–10059.
33 M. P. Maman, A. S. Nair, H. Cheraparambil, B. Pathak and S. Mandal, *J. Phys. Chem. Lett.*, 2020, **11**, 1781–1788.
34 W. W. Xu, B. Zhu, X. C. Zeng and Y. Gao, *Nat. Commun.*, 2016, **7**, 13574.
35 M. G. Taylor and G. Mpourmpakis, *Nat. Commun.*, 2017, **8**, 15988.
36 L. D. Plath, H. Abroshan, C. Zeng, H. J. Kim, R. Jin and M. E. Bier, *J. Am. Soc. Mass Spectrom.*, 2022, **33**, 521–529.
37 S. Theivendran and A. Dass, *Langmuir*, 2017, **33**, 7446–7451.
38 A. Dass, A. Stevenson, G. R. Dubay, J. B. Tracy and R. W. Murray, *J. Am. Chem. Soc.*, 2008, **130**, 5940–5946.
39 P. R. Nimmala and A. Dass, *J. Am. Chem. Soc.*, 2011, **133**, 9175–9177.
40 G. Kresse and J. Hafner, *Phys. Rev. B*, 1994, **49**, 14251–14269.